ELSEVIER

Journal of Molecular Catalysis A: Chemical 162 (2000) 51–66

JOURNAL OF MOLECULAR CATALYSIS A: CHEMICAL

www.elsevier.com/locate/molcata

Complex model catalysts under UHV and high pressure conditions: CO adsorption and oxidation on alumina-supported Pd particles

T. Dellwig, J. Hartmann, J. Libuda *, I. Meusel, G. Rupprechter [1], H. Unterhalt, H.-J. Freund

Fritz-Haber-Institut der Max-Planck-Gesellschaft, Faradayweg 4-6, D-14195 Berlin, Germany

Abstract

The growth of metal particles on ordered oxide surfaces provides a strategy to prepare well-defined model systems for supported catalysts, which can by easily studied by most surface-science techniques. Here, we focus on Palladium particles grown on an ordered Al_2O_3 film on NiAl(110), a system which has previously been characterized in detail with respect to its structural, electronic and adsorption properties.

In this contribution, we will provide several examples, showing how adsorption and reactivity phenomena on these systems can be addressed over a pressure range from ultrahigh vacuum (UHV) to near atmospheric pressure. In the low pressure region, we apply a combination of molecular beam methods and in-situ infrared reflection absorption spectroscopy (IRAS). For CO adsorption, angular resolved scattering and sticking coefficient measurements and structural information allow us to quantify different adsorption channels including reverse spillover effects. The coverage dependent kinetics of CO oxidation is derived and discussed in comparison with the single crystal kinetics.

The adsorption of CO on alumina supported Pd aggregates at low and high pressure, i.e. from 10^{-7}–200 mbar, is examined by IR–VIS sum frequency generation (SFG) vibrational spectroscopy. At low pressure, the CO adsorption site distribution (bridged vs. on-top) depends on the particle surface structure and temperature, but under reaction conditions, the site occupancy is mainly governed by the CO pressure. The impact of these results on the extrapolation of UHV data to high pressure catalysis is discussed.

Keywords: Carbon monoxide; Adsorption; Oxidation; Palladium; Alumina; Molecular beams; Sum frequency generation; Vibrational spectroscopy; High pressure

1. Introduction

It is well documented that the kinetics of heterogeneously catalyzed reactions on supported metals may sensitively depend on a number of parameters such as particle size and structure [1], support material and surface structure or various promoters and poisons ([2] and refs. therein). Many concepts have been put forward to explain these observations, such as size effects altering the electronic properties of small metal particles, geometrical effects due to the presence of characteristic adsorption sites on the particle [3] or at the boundary [4], metal-support

* Corresponding author. http://www.fhi-berlin.mpg.de.
E-mail addresses: libuda@fhi-berlin.mpg.de (J. Libuda), rupprechter@fhi-berlin.mpg.de (G. Rupprechter).
[1] Also corresponding author.

1381-1169/00/$ - see front matter
PII: S1381-1169(00)00321-6

interactions [5–7], support effects involving spillover or reaction on the support ([8] and refs. therein). Also, effects like the coupling between non-equivalent adsorption sites by diffusion have to be taken into account [9,10]. Still, the examples are rare, where the role of these effects has unambiguously and quantitatively been identified on a molecular level (see [11] and refs. therein).

The reasons for this lack of understanding are obvious, yet difficult to overcome. Single crystal studies are principally not capable of reproducing these effects, while technical catalysts are generally too complex to clearly identify the molecular origin. A possible solution to this so-called "material gap" [12] is the development of supported model catalysts [11]. Keeping the system as simple as possible, these models open the possibility to introduce certain complex properties of real catalysts, and — most importantly — they are still easily accessible for most surface science probes.

Several types of supported metal model catalysts have been developed recently (see [11] and refs. therein). Among these are e.g. metal deposits, prepared under well-controlled conditions in ultrahigh vacuum (UHV) on oxide single-crystals or on thin ordered oxide films. The latter may be prepared by metal deposition and oxidation on an inert support [13] or by oxidation of a metal single crystal [14]. We have extensively characterized a variety of such systems with respect to their growth properties, geometric and electronic structure, as well as their adsorption behavior. Extensive reviews on this work can be found in the literature [14,15]. Here, we will choose one particular system — palladium particles supported on a thin ordered alumina film — and discuss how such a system can be utilized to investigate questions typical for supported metal catalysts. A short summary of the structural properties of the system under discussion is given in Section 2, more detailed information can be found in the literature [16–18].

Once the structural properties of a model system are well understood, in the next step new aspects become important. We would like to specifically address two of those questions: (1) how correlations between the structural properties and the microscopic kinetics of a reaction can be established and (2) how spectroscopic studies can be extended from the low pressure range typical for surface science to the catalytically relevant pressure region.

(1) Concerning investigations of microscopic reaction kinetics, molecular beam techniques represent the method of choice [19,20]. With a maximum of control over the reactant flux and its dynamic properties, we can take advantage of the single scattering conditions of a beam experiment to establish reaction mechanisms or determine exact probabilities, rate constants and activation barriers for surface processes. Also, questions of adsorption and reaction dynamics can be addressed [21,22]. In spite of the numerous examples for the application of beam methods to the reaction kinetics on single crystal surfaces, similar studies on more complex surfaces are scarce and limited to very few reaction systems [23–26]. In Section 3, we will present basic examples, showing how the adsorption and reaction kinetics on supported model catalysts can be investigated combining molecular beam methods, gas phase detection and in-situ vibrational spectroscopy.

(2) Furthermore, fundamental studies applying surface sensitive techniques are generally only carried out at low pressures (below 10^{-6} mbar), due to pressure restrictions of methods based on the scattering or emission of electrons, atoms and ions. However, in-situ studies under reaction conditions applying Raman spectroscopy (in particular by the Knözinger group [27–29]), sum frequency generation (SFG) [30] and other techniques [29] have shown that a high pressure gas environment may change the surface of a catalyst and that the adsorption geometry of an adsorbate might depend on pressure as well. IR–VIS SFG surface vibrational spectroscopy is one of the few surface-sensitive techniques that is able to bridge the "pressure gap". Being a photon-based optical method, SFG can cover the pressure range from UHV to ambient conditions [30]. SFG spectra acquired under UHV can be directly compared with infrared reflection absorption spectroscopy (IRAS) and high-resolution electron energy loss spectroscopy (HREELS) data and, furthermore, SFG allows the in-situ observation of surface species under reaction conditions. While SFG has been repeatedly used to observe adsorbates on single crystals (metal and oxide), on thin oxide films, and on metal foil, the ability of SFG spectroscopy to study gas adsorption on supported Pd nanoparticles was demonstrated

just recently [31]. In Section 4, we demonstrate how SFG spectroscopy can be successfully applied to probe the surface structure of Pd aggregates and to monitor pressure-induced changes of the CO adsorption site distribution.

2. Supported model catalysts based on ordered oxide films

As already mentioned in Section 1, the basic requirements for a supported model catalyst are twofold: First, we need to start from a system, as simple and well-characterized as possible and attempt to reproduce those features of a complex catalyst, which may be of relevance for the effects under discussion. Secondly, we have to guarantee that the model system is still accessible to spectroscopic and microscopic methods, which will yield detailed information on structural and electronic properties and thus will provide a basis for the interpretation of the reaction kinetics.

The first step in the development of this type of model catalyst is the preparation of a clean and ordered oxide surface which may serve as a support. Both, oxide single crystal surfaces [11] and ordered films, prepared by oxidation of single crystals [14] or by evaporation of metals onto a host crystal [13], have been used. Here, we will use an ordered Al_2O_3 film prepared by oxidation of a NiAl(110) single crystal. This film is exceptionally well ordered and the preparation is highly reproducible. Its structure, defect structure and adsorption properties have been subject to previous studies [32,33].

In the second step, the active metal particles are prepared on this model support. This is usually done by evaporation of the corresponding metal under UHV conditions, to a large extent excluding sources of contamination. Detailed studies on the growth behavior and particle structure provide the basis for further investigations concerning the adsorption properties and reactivity of these systems. A variety of metals deposited on Al_2O_3/NiAl(110) has been studied and a review of their geometric and electronic properties can be found in the literature [14,15]. In this contribution, we focus only on the system Pd/Al_2O_3/NiAl(110), and in the following we will summarize some of the most relevant results.

Most importantly, the structure, number density and size of the metal particles can be varied over a large range by applying different growth conditions. Under precise control of the growth parameters such as the substrate temperature, metal amount and flux as well as the defect density of the substrate, it is possible to vary the particle size from only a few atoms to several 10,000 atoms/island [14]. In this work, we will basically choose two types of Pd deposits, in the following denoted as preparation conditions 1 and 2, respectively. Details of the structural parameters and preparation are given in Table 1. Most importantly, the Pd particles of type 1 represent relatively large (3500 atoms/island) and well ordered crystallites (see STM image in Fig. 1a). As schematically shown in Fig. 1b, these crystallites grow in (111) orientation and even show an azimuthal alignment with respect to the oxide support. Preferentially, the particles expose (111) facets and only a small fraction of (100) facets. For compari-

Table 1
Preparation conditions and structural parameters for Pd/Al_2O_3/NiAl(110)

	Preparation conditions 1	Preparation conditions 2
Deposition parameters		
Pd coverage [atoms cm^{-2}]	2.7×10^{15}	2.7×10^{15}
Deposition temperature [K]	300	90
Deposition rate [atoms cm^{-2} s^{-1}]	9×10^{12}	9×10^{12}
Structural parameters		
Island density [cm^{-2}]	$0.8\ (\pm 0.1) \times 10^{12}$ [14]	$1.0\ (\pm 0.3) \times 10^{13}$ [14,15]
Number of Pd atoms/island	~3500	~300
Fraction of support covered by Pd	0.20 (±0.02) [41]	0.7 (±0.1) [41]
Fraction of surface Pd atoms	0.20 (±0.03) [41]	0.5 (±0.1) [41]

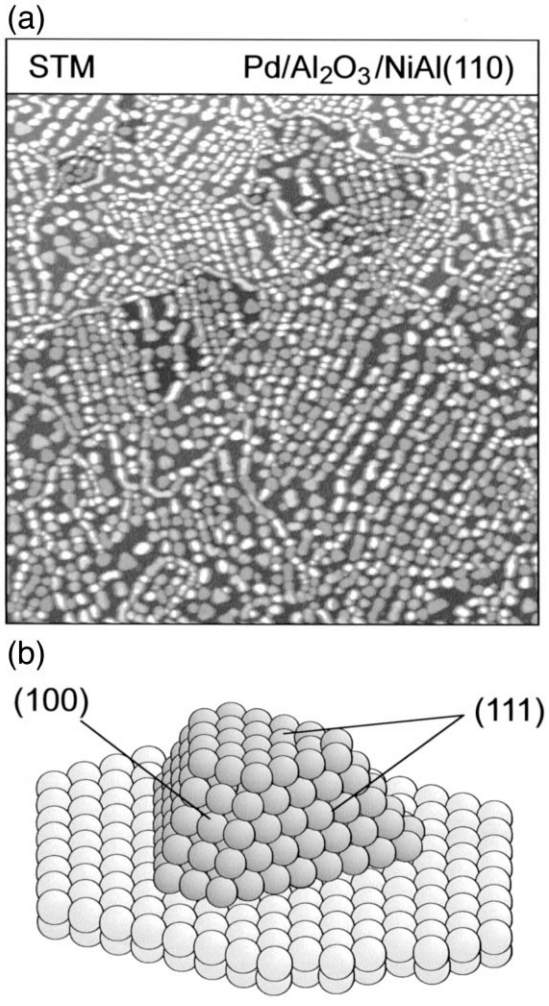

Fig. 1. (a) STM image (CCT, 5000×5000 Å) of Pd particles grown on Al_2O_3/NiAl(110) at 300 K (nominal Pd coverage: 3×10^{15} atoms cm^{-2}), from Ref. [14]; (b) schematic representation of a Pd particle grown on Al_2O_3/NiAl(110) at 300 K.

son, we choose a second type of preparation conditions denoted as Pd particles of type 2. Here, the metal was deposited at lower substrate temperature. The reduced diffusion length under these conditions leads to a higher nucleation density. In comparison to the type 1 case, the particle density is strongly increased, corresponding to a smaller particle size (300 Pd atoms/island) at similar nominal Pd coverage. No indication for the formation of well ordered facets has been found in this case and, consequently, we expect the particle surface to be dominated by a high density of defect sites.

3. Kinetics and spectroscopy at low pressure: molecular beam experiments

Molecular beam methods have established themselves among the most powerful experimental tools to extract detailed quantitative information on the kinetics and dynamics of surface reactions. The main features of the method are the well-defined single-scattering conditions, the high level of control over the dynamic parameters of the reactant beam and the high temporal resolution. In this section, we will present some examples how to derive information addressing the specific adsorption and reaction kinetics on supported metal systems.

3.1. Experimental

The experiments have been performed in a new UHV molecular beam/surface spectroscopy apparatus (base pressure 1×10^{-10} mbar), a detailed description of which can be found elsewhere [34]. It has been specifically designed for kinetic studies on complex model systems.

The sample is prepared in a UHV preparation chamber, by sputtering and annealing of a NiAl(110) single crystal, followed by a subsequent oxidation and annealing procedure. The quality of the oxide film and cleanliness of the sample is checked via Low Energy Electron Diffraction (LEED) and Auger Electron Spectroscopy (AES). Details concerning the oxide film preparation can be found in the literature [32]. Before the actual experiment, the active metal component (Pd) is deposited in UHV under well controlled conditions (2.7×10^{15} atoms cm^{-2} at a sample temperature of 300 K, Pd flux: 9×10^{12} atoms cm^{-2} s^{-1}), which yields the particle density and structure as described in Section 2 (Table 1, preparation conditions 1).

Subsequently, the sample is transferred to the scattering chamber, which contains an experimental setup as depicted schematically in Fig. 2. Up to three

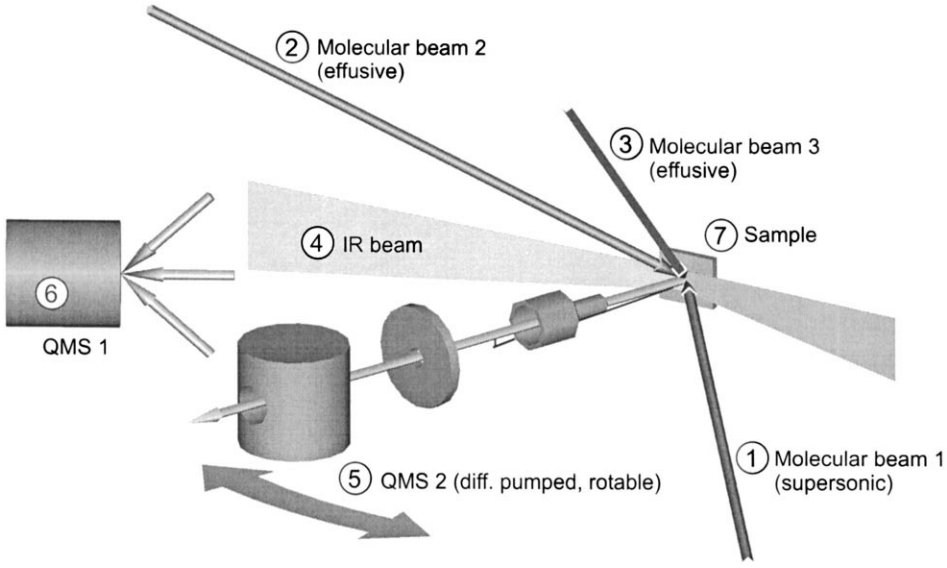

Fig. 2. Schematic representation of the molecular beam experiment.

molecular beams can be crossed on the sample surface providing the reactants. In kinetic studies requiring high reactant fluxes, two modulated effusive sources can be used (Fig. 2, no. 2 and 3), for sticking coefficient measurements or angular resolved scattering a third beam with narrow velocity distribution and well-shaped profile is generated from a supersonic expansion (Fig. 2, no. 1; CO, 3×10^5 Pa). Angular-integrated gas-phase measurements are performed with a quadrupole mass spectrometer (QMS, Fig. 2, no. 6) which is not in direct line-of-sight of the sample. Angular-resolved measurements are realized with a rotatable doubly differentially pumped QMS (Fig. 2, no. 5). Simultaneously, time-resolved IR absorption spectra can be obtained via a vacuum FT-IR spectrometer (Fig. 2, no. 4). A detailed description of the experimental setup and data acquisition procedure can be found elsewhere [34].

3.2. Results and discussion

Generally, the first effect which has to be taken into account in a description of the adsorption or reaction kinetics on supported metal catalysts is substrate mediated adsorption, sometimes also denoted as reverse spillover. The process is schematically illustrated in Fig. 3. An impinging gas molecule may directly collide with the Pd particle with a probability p_{Pd} equal to the Pd coverage and will be adsorbed with a probability $p_{\mathrm{Pd,TA}} = p_{\mathrm{Pd}} S_{\mathrm{Pd}}$ (S_{Pd} is the CO sticking coefficient on Pd, which itself depends on the CO coverage). Alternatively, the molecule may impinge on the substrate (probability p_{S} is equal to the uncovered oxide fraction), be trapped and reach the metal particle via surface diffusion (probability $p_{\mathrm{S,TA}}$). Depending on the diffusion length, this effect may enhance the adsorbate flux to the metal particle considerably and has to be taken into consideration when comparing catalytic activities. Gillet et al. [35] have formulated the effect for CO adsorption on Pd particles. Later, it was taken into account in several adsorption and reaction studies on the same system [23,24,36]. Models have been derived, which allow support diffusion to be taken into account quantitatively in kinetic studies [9,10,37,38]. Experimentally, the necessary model parameters (substrate trapping probability, diffusion length) are usually determined by modeling the temperature dependence of the sticking probability.

In principle, all this information is directly available from a molecular beam experiment. We consider the sticking coefficient $S(\theta)$ ($E_{\mathrm{kin,CO}} =$

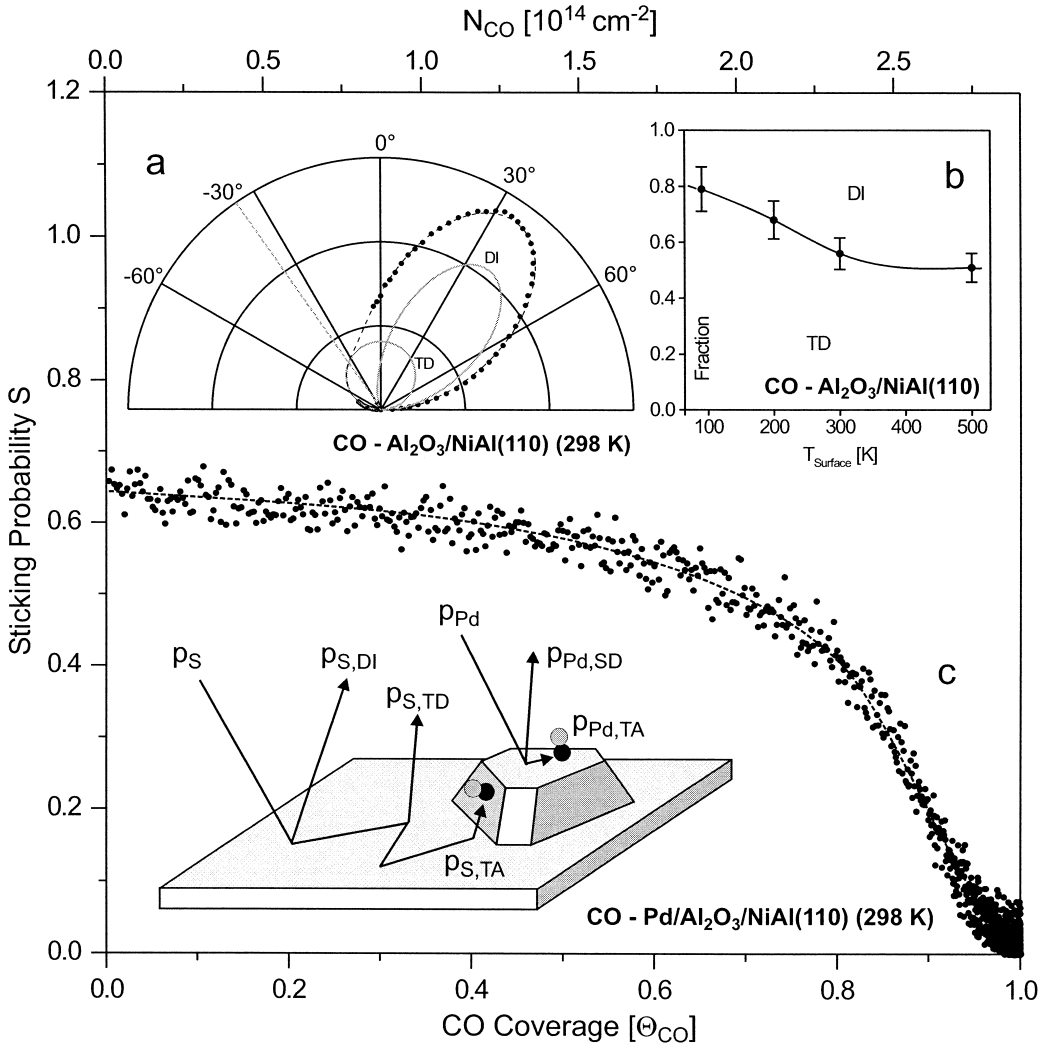

Fig. 3. (a) Angular distribution of CO (kinetic energy 86 meV, incidence angle: $-35°$) scattered from $Al_2O_3/NiAl(110)$; (b) trapping-desorption and direct-inelastic components for CO scattered from $Al_2O_3/NiAl(110)$ as a function of surface temperature; (c) Sticking probability for CO on $Pd/Al_2O_3/NiAl(110)$ (preparation conditions 1, see Table 1); second index: DI: direct-inelastic, TD: trapping-desorption; TA: trapping-adsorption; SD: scattering-desorption.

0.086 eV, $T_{surface} = 298$ K) for the Pd/Al_2O_3 system (Fig. 3c), derived by applying the King and Wells method [39,40]. The corresponding structural parameters are given in Table 1 (preparation conditions 1). Starting from an initial value of $S_0 = 0.64 \pm 0.03$, the sticking coefficient only weakly decreases up to high relative CO coverage; a behavior which is characteristic for precursor mediated adsorption. Only at high coverage the net sticking probability decreases, due to the decreasing probability for finding an unoccupied adsorption site and the decreasing differential adsorption energy resulting in an increasing desorption rate.

In the following, we will consider the limit of low CO coverage as a simple example. Nominally, 20% of the oxide surface are covered by Pd (see Table 1). As discussed in the Section 3.1, the surface of the Pd particles is largely dominated by (111)-facets and the

initial sticking probability for CO on Pd(111) (300 K) has been determined as 0.96 [42]. Thus, we can estimate an initial probability of direct adsorption on the Pd as $p_{Pd,TA} = 0.19$ and for support mediated adsorption a probability of $p_{S,TA} = 0.45$ remains. For CO molecules impinging on the support, three channels should be considered: They may undergo direct scattering ($p_{S,DI}$, direct inelastic (DI) scattering processes dominate under these conditions, see e.g. [21]), they may be trapped and desorb before reaching the metal particle ($p_{S,TD}$), or they may be trapped and diffuse to a Pd particle ($p_{S,TA}$). On the Pd-free alumina support only the DI and TD (trapping desorption) contributions exist (see e.g. [11,21]) and can be identified by angular resolved gas phase detection. The corresponding angular distribution for the scattered CO is shown in Fig. 3a. Now, we assume that the TD component is symmetric with respect to the surface normal (the information on the initial impulse is lost upon accommodation). The information on the incidence angle ($\theta_{in} = -35°$) is largely conserved, however, in the DI contribution. In a polar plot the latter component is represented by a lobe centered around the specular direction ($\theta_{out} = 35°$). The integral fractions of both parts can be estimated by fitting two $\cos^n$-distributions. It has to be pointed out that this procedure represents a simplification, as the trapping process can be significantly more complicated, e.g. due to partial accommodation and inefficient coupling of parallel and perpendicular momentum, see e.g. [21,22], or due to diffuse scattering from defects, see e.g. [11]. However, the first effect is expected to be less important at the low kinetic energies employed here. Regarding the latter, it is found that time of flight (TOF) spectra show a pronounced angular dependence of the kinetic energy, which is expected for the coexistence of the two channels. Assuming we can distinguish between trapping-desorption and direct-inelastic scattering, we obtain an integral surface temperature dependence as depicted in Fig. 3b. With increasing surface temperature the trapping probability decreases from approximately 0.8 at 100 K to 0.5 at 500 K. Very similar values are found for CO on α-alumina [43] and MgO(100) [44]. The temperature dependence is expected for trapping at low kinetic energies and can be easily understood qualitatively: With an increasing fraction of collisions, where the colliding surface atom is moving "outwards", the collisional energy transfer is more likely to become insufficient to facilitate trapping (see e.g. [21,22]).

If we combine this information with the structural data on the system, the probabilities for all processes shown in Fig. 3 have been determined. Applying the estimated trapping probability on the alumina support (0.55 ± 0.05), to the sticking on the Pd/Al_2O_3 system (nominal 80% alumina coverage) we estimate a probability of $p_{S,TD} + p_{S,TA} = 0.44 \pm 0.05$ for CO to be trapped on the support. We can now compare this value with the above number for support mediated adsorption, and we conclude that under these conditions practically all CO molecules trapped on the surface will diffuse to the metal particle and desorption after trapping on the support is negligible ($p_{S,TD} \approx 0$). With increasing surface temperature, desorption from the support will become faster and substrate mediated adsorption will become less effective [45].

From the simple adsorption of molecules, we will now move on to the kinetics of surface reactions. Specifically, we consider the CO oxidation reaction, which is the best studied catalytic reaction in surface science. On Pd(111), this system was early studied by Engel and Ertl [46], who demonstrated via modulated beam methods that the reaction follows a Langmuir–Hinshelwood (LH) mechanism. Although the kinetics of the reaction on Pd single crystal surfaces is rather structure insensitive, certain structure dependencies are found on supported particles. Possible kinetic effects range from e.g. (1) apparent structure sensitivities caused by the substrate adsorption and reverse spillover contribution discussed above to (2) actual structure sensitivities caused by new adsorption sites on small particles, (3) nonlinear diffusion mediated effects, or (4) the possible influence of subsurface oxygen. A detailed discussion is beyond the scope of this paper, but previous work has been extensively reviewed in the literature [11]. Here, we will restrict ourselves to a simple example, which shows how the well-defined single scattering conditions of a beam experiment can be utilized to derive kinetic data.

We will employ the same preparation conditions for the Pd/Al_2O_3 system as in the CO adsorption experiment discussed before (Table 1, preparation conditions 1). In contrast to the adsorption experi-

ments, the Pd particles were stabilized by repeated cycles of O_2 and CO adsorption at 366 K which is necessary to obtain reproducible reaction rates. This stabilization procedure does not change the island density or morphology, but it is related to the formation of subsurface oxygen, as will be discussed elsewhere [47]. After the stabilization procedure and before the actual experiment, the sample is exposed to oxygen (2.0×10^{16} O_2 molecules cm^{-2}). Subsequently, a transient experiment is performed, during which the oxygen precovered sample is exposed to a CO beam (8.6×10^{12} molecules cm^{-2} s^{-1}). The CO sticking coefficient and the CO_2 production rate are measured simultaneously (see Fig. 4, $T_{\mathrm{Surface}} =$ 402 K). Now, the total CO consumption (CO adsorption and oxidation, $N_{\mathrm{CO,total}}$) can be determined by integration of the CO sticking coefficient (Fig. 4b), and the total CO adsorption capacity ($N_{\mathrm{CO},\infty}$) can be derived from a corresponding experiment after thermal CO desorption. The difference between both values is the amount of CO or O ($N_{\mathrm{O},0}$) involved in the reaction. Once those limits are determined, all surface coverages (Fig. 4c) can be derived by integration of the CO_2 production and O_2 adsorption (see e.g. [27,46]). In the next step, we apply a rigorous definition of the LH reaction rate as

$$\frac{\mathrm{d}}{\mathrm{d}t} N_{\mathrm{CO_2(g)}} = k_{N_{\mathrm{CO}},N_{\mathrm{O}}} N_{\mathrm{CO}} N_{\mathrm{O}}$$

to derive the rate constant $k_{N_{\mathrm{CO}},N_{\mathrm{O}}}$. Please note that this rate "constant" may strongly depend on the adsorbate coverage, e.g. due to the coverage dependent spatial distribution of the adsorbed species, adsorbate–adsorbate interactions or the presence of different types of reaction sites. We can, however, derive quantities such as the activation energy for the LH step as a function of the oxygen or CO coverage. This will be discussed in detail elsewhere [48]. Here, we will restrict the discussion to a short comparison with single crystal experiments, illustrating the possible differences between both types of reaction systems. Engel and Ertl [46] have reported a similar experiment on Pd(111). Apparently, the coverage dependence of the rate constant is qualitatively different for alumina supported Pd particles. Contrary to what is found on the single crystal, $k_{N_{\mathrm{CO}},N_{\mathrm{O}}}$ shows a steep drop at high oxygen coverage (Fig. 4c). After consumption of the fast reacting oxygen, the rate constant decreases slowly until it reaches very low values after consumption of approximately 80% of the preadsorbed oxygen. The origin of this effect is not clear yet. A possible explanation is related to the formation of dense oxygen adlayers, which show an increased reaction rate. Similar effects have recently been observed on Pd(100) and Pd(110) films [49,50]. Also, the coexistence of (111) and (100) facets as well as edge sites on the crystallites has to be taken into account. Coupled via surface diffusion, differences in the adsorption properties or rate constants between these types of surface areas may lead to drastic variations in the reaction rate [9,10]. Systematic molecular beam studies, varying the structure and adsorbate coverage of the model systems may — in connection with exact structural information — help to elucidate the origin of such effects.

To complement the gas phase detection, in-situ surface spectroscopic methods can be combined with molecular beam techniques. This is particularly important for complex surfaces, as we gain the possibility to obtain qualitative and quantitative information on different surface species. As a simple example a combined reactivity/IRAS experiment on CO oxidation is shown in Fig. 5. Contrary to the experiment in Fig. 4, we start with the surface being precovered by CO. Via an effusive source oxygen is dosed in pulses of 3.9×10^{14} molecules cm^{-2} $pulse^{-1}$. Simultaneously, the CO_2 production is recorded and an IR spectrum is recorded after each pulse. Here, we will only qualitatively point out the type of information, which is available from this experiment: (1) The envelope over the response pulses corresponds to the O_2 reactive sticking coefficient as a function of CO coverage. As CO has a strongly inhibiting effect on the adsorption of oxygen [46], the sticking coefficient and thus the CO_2 production is initially low. Both quantities increase with decreasing CO coverage. (2) Every CO_2 response pulse shows a rise and decay time slower than the originating O_2 pulse (which is rectangular on the time scale of the experiment). The extraction of kinetic data from such time resolved measurements is one of the standard methods to derive kinetic parameters [19,20]. (3) Last but not least, information on the coverage dependent occupation of adsorption sites is available from the IR spectra (Fig. 5). The left series of IR spectra represent the total CO consumption (reference spec-

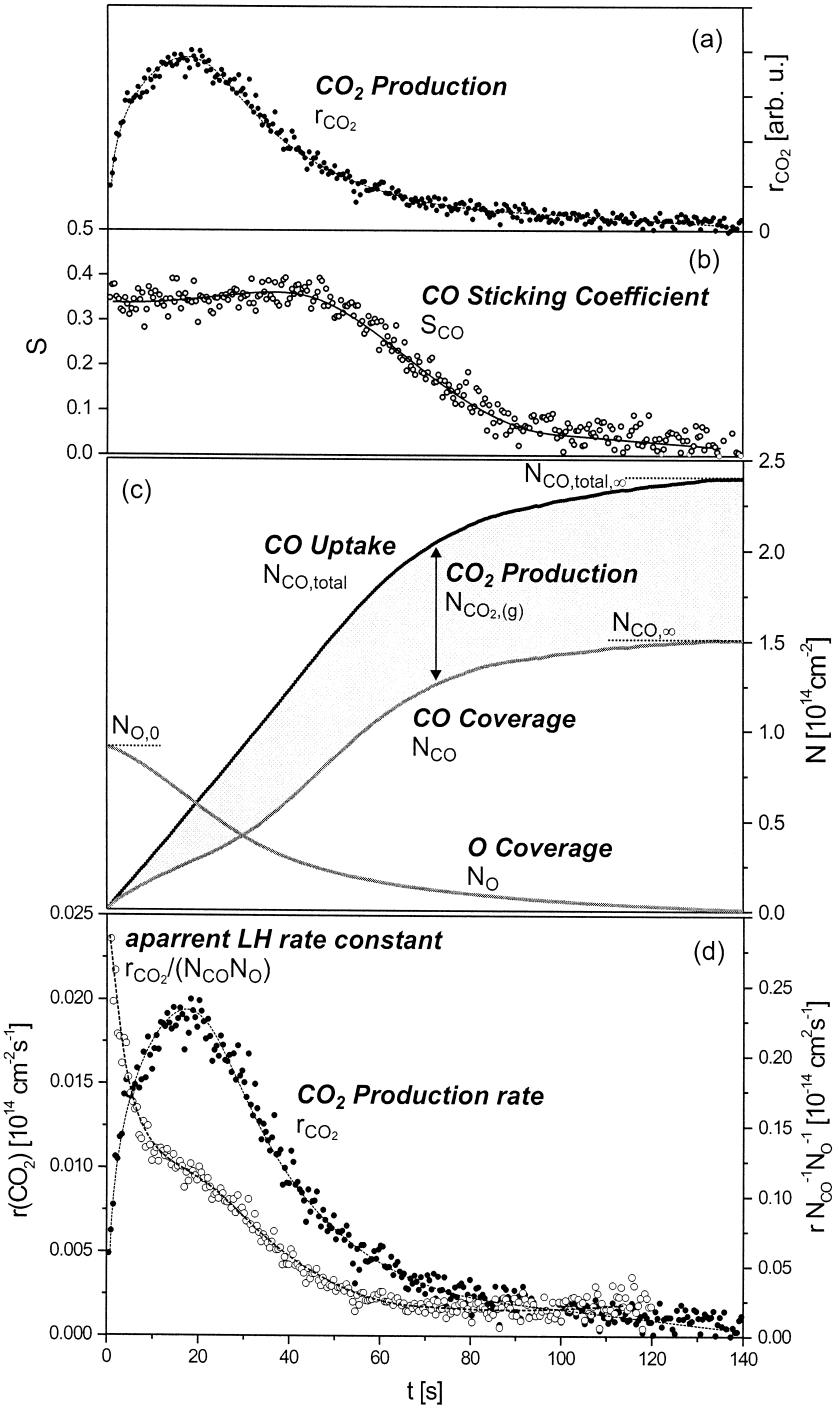

Fig. 4. (a) Relative CO_2 production for O-precovered $Pd/Al_2O_3/NiAl(110)$ at a sample temperature of 402 K (preparation conditions 1, CO beam: 8.6×10^{12} molecules cm^{-2} s^{-1}), (b) CO sticking coefficient as a function of experiment time; (c) O and CO surface coverages (see text); (d) absolute CO_2 production rate and apparent LH rate constant.

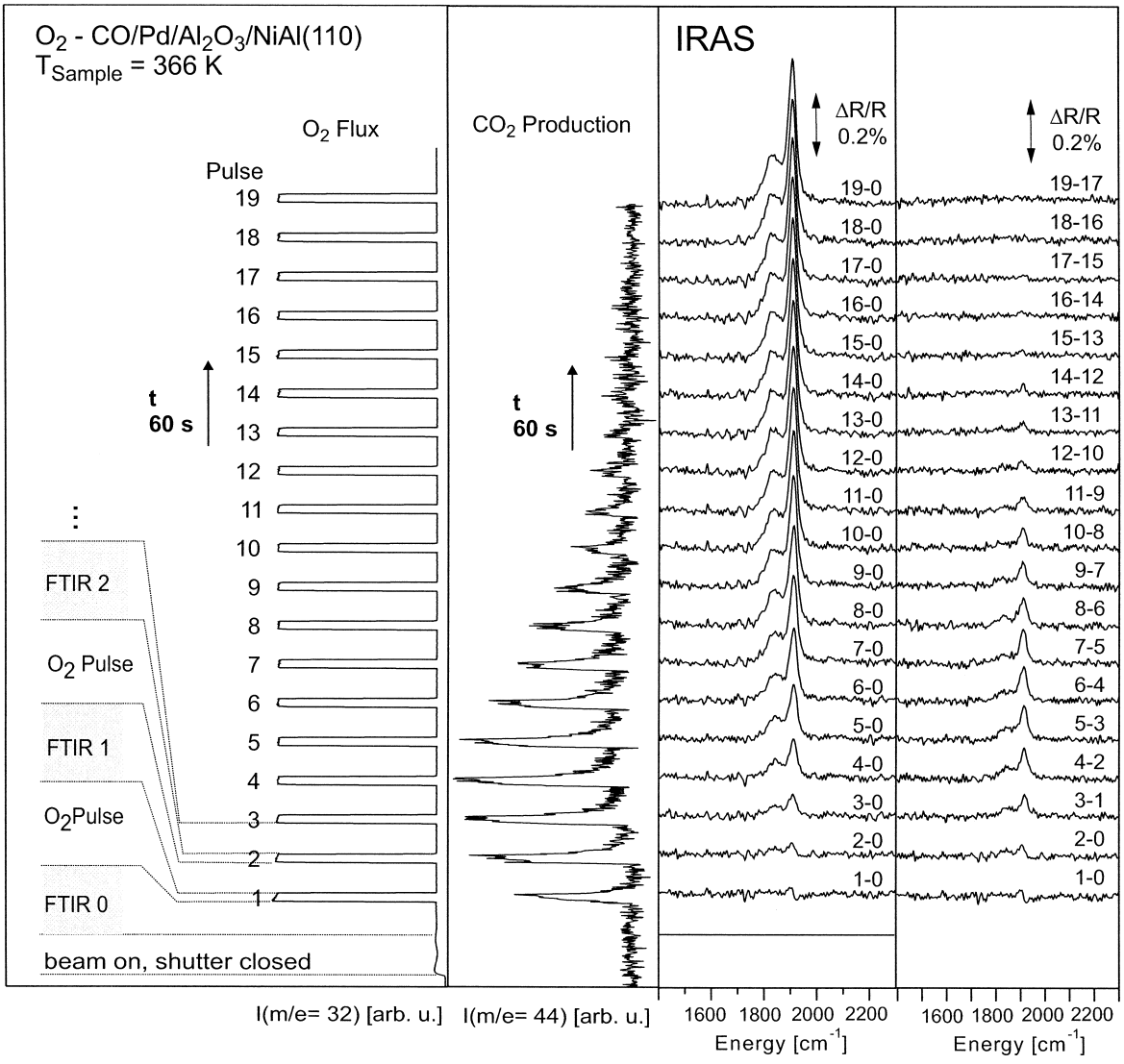

Fig. 5. Correlated reactivity/IR absorption experiment: O_2 is pulsed on CO-precovered $Pd/Al_2O_3/NiAl(110)$ (preparation conditions 1, sample temperature 366 K). From left to right: (1) O_2 partial pressure, (2) CO_2 production (background corrected), (3) IR absorption spectra relative to the CO saturated system, (4) differential IR absorption spectra.

trum is the CO saturated spectrum). Alternatively, the differential CO consumption can be derived by calculating the difference between adjacent spectra (right series, Fig. 5). A detailed discussion of the IR spectra for this system can be found in the literature [18]. Shortly, we can distinguish between CO bound in bridge (1910 cm^{-1}) and higher coordinated sites (1830 cm^{-1}) and identify possible changes in the ratio of both species in the course of the experiment [48]. This example shows how well controlled reactivity studies via molecular beam methods can be successfully correlated with in-situ spectroscopy. We expect that this type of combined information will be of great importance in future attempts to identify to origin of the special kinetics of surface reactions on complex supported catalysts.

4. Spectroscopy at low and high pressure: sum-frequency generation

Applying SFG surface vibrational spectroscopy to a well-defined but complex model catalyst of Pd nanoparticles on an ordered alumina film allows to simultaneously bridge both the pressure and materials gaps in heterogeneous catalysis [31]. SFG spectroscopy can be carried out over a wide pressure range, i.e. from UHV to near ambient conditions, and it was previously utilized to study a variety of adsorbates on metal and oxide single crystal surfaces at low and high pressure [30,51,52]. Furthermore, SFG was carried out on thin epitaxial oxide films [53], and on polycrystalline metal foil [54]. Although the applicability of SFG spectroscopy to nanostructured supported catalysts has been questioned for several reasons (scattering of laser beams on rough surfaces, disordered adsorbates, small total coverages, etc.), we recently succeeded to obtain SFG spectra from CO adsorbed on supported Pd nanoclusters [31]. The structural order and the "flatness" of the supporting alumina film, its very small thickness, and the mean size of the Pd particles that is well below the wavelength of the incident light allowed to circumvent the restrictions mentioned above.

In this study, we apply SFG spectroscopy to follow CO adsorption on supported Pd nanoparticles over a wide pressure (10^{-7}–200 mbar) and temperature (190–300 K) range. The CO adsorption site occupancy on Pd nanocrystals turns out to be different from single crystals. In addition, it is mainly determined by the CO gas phase pressure while the structure of the particles and their temperature have a smaller influence.

4.1. IR–VIS SFG vibrational spectroscopy

Vibrational spectroscopies have been proven to be among the most powerful techniques to study the interaction of gas molecules with metal surfaces. In many cases, e.g. CO adsorption on noble metals, the observed CO stretching frequency can be correlated with a specific binding site [55] (with the exception of more complex (coadsorption) systems as shown by photoelectron diffraction [56]). The SFG process has been reviewed in detail in the literature ([30,51,57] and refs. therein). Briefly, SFG is a second-order nonlinear optical process which involves the mixing of tunable infrared (ω_{IR}) and visible light (ω_{VIS}) to produce a sum frequency output ($\omega_{SFG} = \omega_{IR} + \omega_{VIS}$) (Fig. 6). Since the SFG process is only allowed in a medium without inversion symmetry (in the electric dipole approximation), it can only occur at surfaces (or interfaces) as here the inversion symmetry is broken. Consequently, the dominant contribution to the SFG signal is generated by the modes of the adsorbate, while the centrosymmetric bulk of face-centered cubic metals and an isotropic gas phase give nearly zero contribution to the signal. To obtain an SFG vibrational spectrum of adsorbate molecules on a metal catalyst surface, two ps-laserpulses are spatially and temporally overlapped on the sample (Fig. 6). One input beam is in the visible range at fixed frequency, while the second one is tunable in the infrared to probe the vibrational modes of the surface species. By tuning the IR beam and monitoring the intensity of the SFG output, an adsorbate vibrational spectrum is obtained by plotting the SFG intensity vs. the IR wavenumber. All experiments were made in (p,p,p) geometry, i.e. all beams were p-polarized [30].

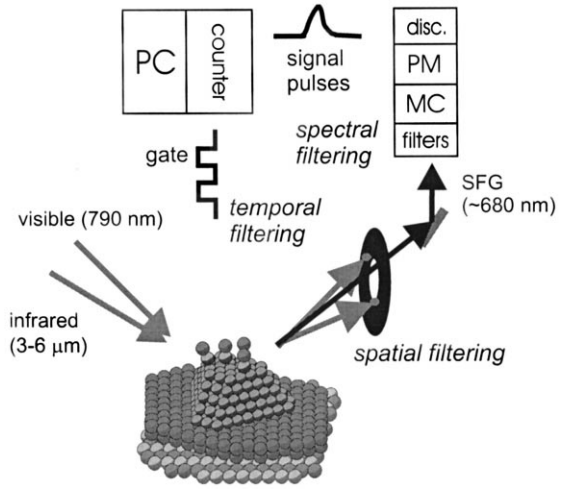

Fig. 6. Illustration of the sum frequency generation process on alumina supported Pd aggregates. The detection system employs spatial, spectral and temporal filtering of the SFG signal (MC: monochromator; PM: photomultiplier; disc.: discriminator).

4.2. Experimental

The experiments were carried out in a new custom-designed apparatus that allows to prepare and characterize supported nanoparticles under well-controlled conditions in UHV (base pressure 1×10^{-10} mbar), to transfer the sample to an SFG-compatible UHV-high pressure cell, and to monitor gas adsorption from submonolayer coverages up to several 100 mbar by SFG vibrational spectroscopy. A detailed description of the chamber is given elsewhere [58]. Samples can be moved from UHV to the high pressure cell using a 400 mm z-travel manipulator. A sample holder that is connected to the manipulator allows resistive heating of the sample (1300 K), cooling with liquid N_2 (85 K), and temperature readings using a chromel–alumel thermocouple. The high and low pressure sections are separated by an arrangement of three differentially pumped spring-loaded Teflon seals. When the SFG cell is pressurized to 1 bar, a vacuum of 5×10^{-10} mbar can be maintained in the preparation/surface analysis chamber.

Supported Pd nanoparticles were prepared following the procedure that was described in Section 2 [14]. An ordered aluminum oxide film was grown on NiAl(110) by oxidation in 10^{-5} mbar oxygen at 523 K and Pd was subsequently deposited by electron beam evaporation. Pd particles of 4 nm mean size ($\sim$ 300 atoms per particle, particle density $\sim 10^{13}$/cm^2, preparation conditions 2, Table 1) were grown at 90 K, and Pd particles with 7 nm mean size ($\sim$ 3500 atoms/particle, particle density $\sim 8 \times 10^{11}$/cm^2, preparation conditions 1, Table 1) were grown at 300 K. The influence of the preparation parameters on the size and morphology of metal aggregates has been studied in detail with STM and SPA-LEED [14–16]. The surface structure and cleanliness of the sample surfaces were examined by LEED, AES, and TPD.

For vibrational studies, the Pd/Al_2O_3 catalysts were transferred under UHV into the SFG-compatible reaction cell. The SFG cell is equipped with two CaF_2 windows to allow the infrared and visible beams to enter, and to allow sum frequency radiation to exit to the detection system. The infrared and visible beams make an angle of about 55° and 50° with respect to the surface normal, respectively, and overlap at the sample surface. The difference in the incident angles of the beams is necessary to spatially separate the SFG signal from the reflected pump beams (cf. Fig. 6). The source of the visible radiation (790 nm, 2 mJ/pulse, 2 ps, 500 Hz) is an amplified titanium sapphire laser (Spectra Physics), and 90% of the output is used to generate tunable infrared light (3–6 μm, ca. 10 μJ/pulse) with an optical parametric generator/amplifier (OPG/OPA; Light Conversion). The infrared power is nearly constant between 2000 and 3300 cm^{-1}, but decreases below 2000 cm^{-1} due to a reduction of the transmission of the $AgGaS_2$ crystal in the OPG/OPA. CO is introduced via a manifold after passing a cold trap that removes carbonyl impurities and the gas pressure is measured using a Baratron gauge. To apply low exposures in UHV experiments, a leak valve and an ionization gauge are also attached to the reactor.

It was mentioned in Section 4.1 that the SFG process is insensitive to the gas phase. However, the absorption of infrared light at high CO pressure must be considered. The intensity of the SFG signal depends on the intensity of the IR-pulse, which may be attenuated and modulated by gas phase absorption. In order to normalize our SFG spectra and to compensate for gas phase absorption, we acquired SFG spectra of a GaAs reference crystal between 10^{-7} and 200 mbar CO [58]. Since the zincblende structure of GaAs exhibits no inversion symmetry, GaAs should produce a constant SFG signal and any variation in the SFG signal hence originates from gas phase absorption of the IR beam. Using these compensation curves, the high pressure SFG spectra were corrected for gas phase absorption. The IR frequency was calibrated to an accuracy of ± 3 cm^{-1} by measurements of the atmospheric CO_2 absorption bands around 2350 cm^{-1}.

4.3. Results and discussion

SFG vibrational spectra of CO adsorbed on Pd/Al_2O_3 at 190 K are presented in Fig. 7a. The mean size of the Pd particles was 4 nm and spectra were taken at 10^{-7}, 10^{-3}, 1, 10, 100 and 200 mbar. The 10^{-7} mbar CO SFG spectrum of the 4 nm Pd particles (preparation conditions 2, Table 1) is nearly identical to the corresponding IRAS spectrum ac-

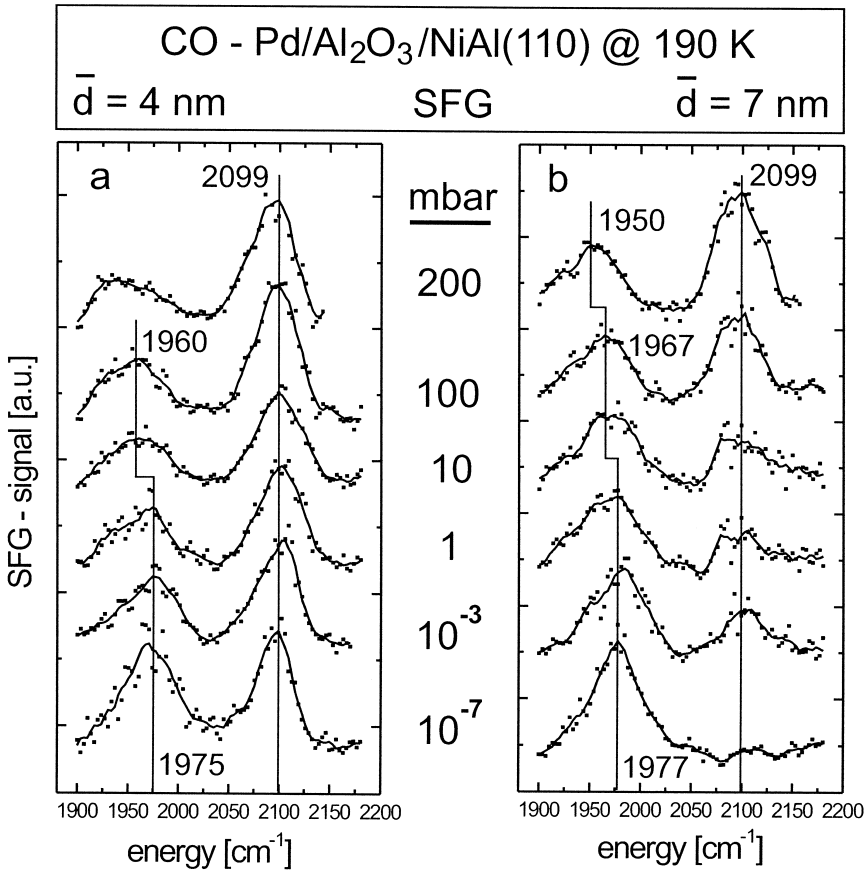

Fig. 7. SFG spectra of CO adsorption on Pd/Al_2O_3 at 190 K between 10^{-7} and 200 mbar: (a) 4 nm Pd particles grown at 90 K and (b) the corresponding SFG spectra acquired on larger and well-facetted supported Pd particles (7 nm Pd particles grown at 300 K). At low pressure the fraction of terminal CO is smaller on the more ordered 7 nm Pd particles as compared to the 4 nm Pd particles.

quired on the same model system at saturation coverage of CO [18]. Based upon IRAS results on Pd single crystals [55,59,60], the two peaks are identified as bridge bonded CO at 1975 cm^{-1} and as terminal (on-top) CO at 2099 cm^{-1}. If the integrated SFG signal intensity is used to determine the ratio of on-top to bridged CO, a value of about 0.8 is obtained. It should be noted that this value is only an estimate because the SFG intensity can not be easily correlated with the surface concentration of a species [30]. However, the adsorption site distribution on the 4 nm Pd aggregates is certainly different from Pd single crystals. On the nanoparticles, bridge bonded CO is accompanied by a significant fraction of terminal CO, a situation which is not apparent on Pd single crystals [55,59,60]. For coverages below 0.5, adsorption in threefold-hollow sites dominates on Pd(111). We could not observe CO adsorption at hollow sites since the frequency range below 1900 cm^{-1} is not accessible by our current SFG setup. For coverages of about $\Theta = 0.5$–0.65, CO is predominantly bridge bonded (1920–1970 cm^{-1}) but the amount of terminally bonded CO is nearly zero. As reported by Tüshaus et al. [59] for Pd(111), the onset of CO adsorption in terminal geometry is at coverages > 0.6. At saturation coverage ($\Theta = 0.75$), two strong bands are observed at 2110 and 1895 cm^{-1} which were assigned to terminally bonded CO and to CO adsorbed on threefold-hollow sites. However, at high coverage the population of bridge sites on Pd(111) is again very small. The coexistence of bridge and on-top CO is presumably due to defects on the 4 nm Pd particles. In fact, the site distribution on the Pd aggregates compares best with defect

rich single crystal Pd(111) or rough Pd thin films [55,59,61]. The peak frequencies also agree well with those observed on 7.5 nm Pd particles on silica prepared by impregnation [62], and with alumina [63] and titania [64] supported Pd model catalysts. The difference between supported Pd clusters and Pd(111) presumably results from a reduced lateral CO interaction on the nanoparticles or from the presence of additional crystal planes. Taking into account the disordered structure of Pd particles grown at 90 K, it seems reasonable that the feature at 1975 cm^{-1} originates from CO bridge-bonded to defect or edge sites. Increasing the pressure above 1 mbar CO shifted the frequency of the bridge peak (Fig. 7a) and also the ratio of on-top vs. bridge CO was increased (10^{-3} mbar: 1.2; 1 mbar: 1.5; 10 mbar: 1.6; 100 mbar: 1.7; 200 mbar: 1.9). The 10^{-7} mbar spectrum could be reproduced after the high gas pressure was pumped out and no indications for particle disrupture upon CO exposure were observed.

In order to study the effect of increasing the particle size and order, the same experiment was carried out on well-facetted Pd particles of 7 nm mean size (preparation conditions 1, Table 1) grown at 300 K (Fig. 7b, cf. Fig. 1b). Only a very small fraction of on-top CO (< 0.1) was detected at 10^{-7} mbar, assuming that the relation between the SFG intensity and the surface concentration of CO is similar on 4 and 7 nm Pd particles. Apparently, adsorption at on-top sites is more pronounced on small defective aggregates as compared to larger and well-facetted Pd nanocrystals. Taking into account the particle morphology (Fig. 1b), it seems unlikely that CO adsorption on Pd(100) contributes to the spectrum since these facets are present only in a small fraction. In our previous IRAS study [18], different frequency regimes were assigned to bridge bonded CO on the terraces of the Pd aggregates (1930–1970 cm^{-1}) and to bridge bonded CO on the edges of the aggregates (1970–2000 cm^{-1}). The resolution of our current SFG prevents a clear discrimination between the two bridge-bonded CO species, but small shoulders on the bridge peaks of the 7 nm Pd particles might indicate the presence of a second component.

If the spectra of the 4 and 7 nm Pd particles at 10^{-7} mbar are compared, it is evident that the adsorption site distribution is quite different. As already mentioned, the defective structure of the 4 nm particles (grown at 90 K) allows more top-site adsorption, while on the 7 nm particles bridged CO dominates. If this result is simply extrapolated to the high pressure regime, one is tempted to explain any difference in the catalytic activity of the 4 and 7 nm Pd particles by the different adsorption site distribution. However, as will be shown below, this assumption is incorrect.

If the CO pressure is increased on the 7 nm Pd particles (Fig. 7b), the relative ratio of on-top CO approaches about the same value as observed for the 4 nm Pd particles (10^{-3} mbar: 0.5; 1 mbar: 0.5; 10 mbar: 0.7; 100 mbar: 1.2; 200 mbar: 1.7). This indicates that the adsorption site distribution at high pressure (e.g. 200 mbar) is independent of particle size, at least for the size range studied.

Of course, catalytic reactions are generally carried out not only at high pressures but at high temperatures as well. Therefore, a second set of experiments was performed at 300 K. This is still a rather low temperature but it is sufficient to drastically change the adsorption behavior. If the sample temperature is raised to 300 K, which is above the desorption temperature of on-top CO on Pd clusters [14], bridge-bonded CO is the only species that can be observed by SFG at 10^{-7} mbar for both 4 and 7 nm Pd particles (Fig. 8; the corresponding spectra for 4 nm Pd particles are nearly identical). However, with increasing pressure, the on-top adsorption sites can be re-populated and an on-top CO ratio as high as 0.8 can be obtained (1 mbar: 0.5; 10 mbar: 0.5; 100 mbar: 0.6; 200 mbar: 0.8; as measured by SFG).

The SFG spectra clearly indicate that the adsorption site occupancy of CO on 4 and 7 nm Pd/Al_2O_3 is mainly governed by the CO pressure and that the influence of particle size, structure (growth conditions) and temperature is less important (at least for the conditions studied here). If these catalysts show a different catalytic behavior at high pressure, it is presumably due to the effects listed in the introduction (metal-support interaction, electronic structure, etc.) but not due to significant differences in the adsorption site distribution.

The combination of SFG spectroscopy and a well-defined nanocluster model catalyst allows to bridge the pressure and materials gaps simultaneously. Low pressure results cannot be simply extrap-

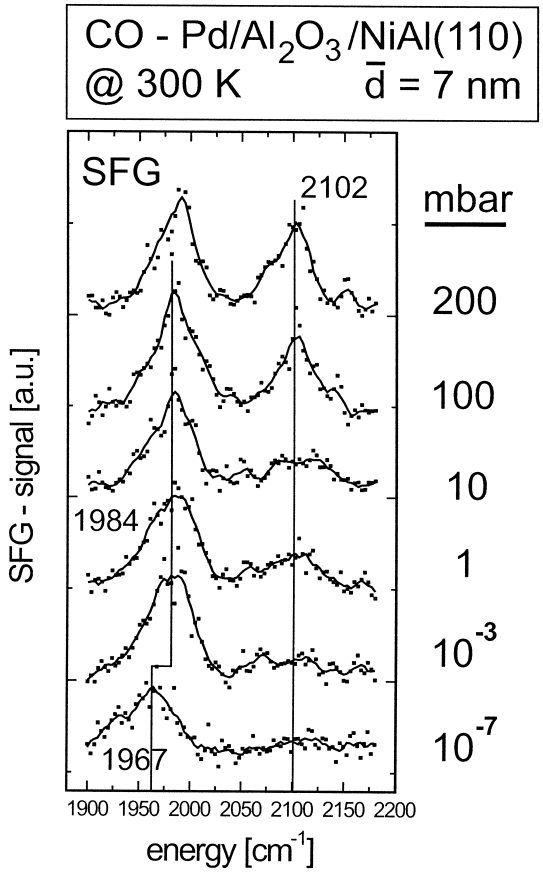

Fig. 8. SFG spectra of CO adsorption on a Pd/Al_2O_3 model catalyst at 300 K (7 nm Pd particles grown at 300 K). Terminal CO sites are re-populated at ≥ 1 mbar.

olated to reaction conditions (although this may be adequate for some adsorbate systems [58]). The pressure dependent site occupation of Pd particles at 300 K clearly reveals the limitation of studies that only consider low pressure. In the near future, we will also apply SFG spectroscopy to study adsorbates during catalytic reactions.

5. Conclusions

We have presented several examples which show how supported model catalysts can be utilized (1) to investigate correlations between structural properties and microscopic kinetics of a surface reaction and (2) to monitor adsorbates from UHV pressures typical for surface science up to the catalytically relevant pressure region. As a model system, we have chosen the CO adsorption and oxidation on Pd particles supported on a well-ordered alumina film, grown on NiAl(110).

Concerning the CO oxidation in the low temperature region, we discuss the application of transient molecular beam techniques with respect to the determination of reaction rates. As an example for a process specific for supported model catalysts, substrate mediated adsorption is considered. It is shown, how the different adsorption/desorption channels can be distinguished, taking advantage of the single-scattering conditions of a beam experiment. Finally, an example for simultaneous in-situ IR spectroscopy and gas phase detection in a transient beam experiment is presented.

We have demonstrated the ability of in-situ SFG spectroscopy to study CO adsorption on supported Pd nanoparticles over a wide pressure (10^{-7}–200 mbar) and temperature (190–300 K) range. The adsorption site occupancy (bridge vs. on-top CO) is considerably different at low and high gas pressure. While under UHV conditions the site distribution depends on the particle surface structure and temperature, under reaction conditions, it is mainly governed by the CO pressure. By exposing Pd/Al_2O_3 to CO pressures ≥ 1 mbar on-top sites that are not filled under UHV can be repopulated and hence contribute to the catalytic turnover.

Combining the data obtained from molecular beam experiments and SFG spectroscopy will provide a wealth of information over a wide range of pressure and temperature and should considerably improve our understanding of catalytic processes.

References

[1] M. Che, C.O. Bennett, Adv. Catal. 36 (1989) 55.
[2] Z. Paál, G. Somorjai, in: G. Ertl, H. Knözinger, J. Weitkamp (Eds.), Handbook of Heterogeneous Catalysis vol. 3, VCH, Weinheim, 1997.
[3] C. Becker, C.R. Henry, Catal. Lett. 43 (1997) 55.
[4] K. Hayek, R. Kramer, Z. Paál, Appl. Catal., A 162 (1997) 1.
[5] G. Paccioni, N. Rösch, Surf. Sci. 306 (1994) 169.
[6] S. Ogawa, S. Ichikawa, Phys. Rev. B 51 (1995) 17231.
[7] G. Rupprechter, G. Seeber, H. Goller, K. Hayek, J. Catal. 186 (1999) 201.

[8] G.M. Pajonk, in: G. Ertl, H. Knözinger, J. Weitkamp (Eds.), Handbook of Heterogeneous Catalysis vol. 3, VCH, Weinheim, 1997.
[9] V.P. Zhdanov, B. Kasemo, J. Catal. 170 (1997) 377.
[10] V.P. Zhdanov, B. Kasemo, Surf. Sci. 405 (1998) 27.
[11] C.R. Henry, Surf. Sci. Rep. 31 (1998) 121.
[12] D.W. Goodman, Surf. Rev. Lett. 2 (1995) 9.
[13] D.R. Rainer, D.W. Goodman, J. Mol. Catal. A 131 (1998) 259.
[14] M. Bäumer, H.-J. Freund, Prog. Surf. Sci. 61 (1999) 127.
[15] M. Bäumer, J. Libuda, H.-J. Freund, Chemisorption and reactivity on supported clusters and thin films, in: M. Lambert, G. Pacchioni (Eds.), NATO — Advanced Study Institute, NATO ASI Ser. E, Kluwer Academic Publishing, 1997, p. 61.
[16] K.H. Hansen, T. Worren, S. Stempel, E. Laegsgaard, M. Bäumer, H.-J. Freund, F. Besenbacher, I. Stensgaard, Phys. Rev. Lett. 83 (1999) 4120.
[17] M. Bäumer, J. Libuda, A. Sandell, H.-J. Freund, G. Graw, T. Bertrams, H. Neddermeyer, Ber. Bunsen. Phys. Chem. 99 (1995) 1381.
[18] K. Wolter, O. Seiferth, H. Kuhlenbeck, M. Bäumer, H.-J. Freund, Surf. Sci. 399 (1998) 190.
[19] M. Asscher, G.A. Somorjai, in: G. Scoles (Ed.), Atomic and Molecular Beam Methods vol. 2, Oxford Univ. Press, 1988, p. 489.
[20] M.P.D. Evelyn, R.J. Madix, Surf. Sci. Rep. 3 (1984) 413.
[21] C.T. Rettner, D.J. Auerbach, J.C. Tully, A.W. Kleyn, J. Phys. Chem. 100 (1996) 13021.
[22] J.A. Barker, D.J. Auerbach, Surf. Sci. Rep. 4 (1985) 1.
[23] C. Becker, C.R. Henry, Surf. Sci. 352 (1996) 457.
[24] C. Becker, C.R. Henry, Catal. Lett. 43 (1997) 55.
[25] I. Stará, V. Nehasil, V. Matolín, Surf. Sci. 331 (1995) 173.
[26] I. Stará, V. Nehasil, V. Matolín, Surf. Sci. 365 (1996) 69.
[27] H. Knözinger, G. Mestl, Top. Catal. 8 (1999) 45.
[28] G. Mestl, H. Knözinger, in: G. Ertl, H. Knözinger, J. Weitkamp (Eds.), Handbook of Heterogeneous Catalysis vol. 2, Wiley-VCH, Weinheim, 1997, p. 539.
[29] J.M. Thomas, G.A. Somorjai (Eds.), Top. Catal. vol. 8, 1999, special issue on "In-situ Characterization of Catalysts".
[30] G.A. Somorjai, G. Rupprechter, J. Phys. Chem. B 103 (1999) 1623.
[31] T. Dellwig, G. Rupprechter, H. Unterhalt, H.-J. Freund, Phys. Rev. Lett. 85 (2000).
[32] R.M. Jaeger, H. Kuhlenbeck, H.-J. Freund, M. Wuttig, W. Hoffmann, R. Franchy, H. Ibach, Surf. Sci. 259 (1991) 235.
[33] J. Libuda, F. Winkelmann, M. Bäumer, H.-J. Freund, Th. Bertrams, H. Neddermeyer, K. Müller, Surf. Sci. 318 (1994) 61.
[34] J. Libuda, I. Meusel, J. Hartmann, H.-J. Freund, Rev. Sci. Instrum., accepted for publication.
[35] E. Gillet, S. Channakhone, V. Matolin, M. Gillet, Surf. Sci. 152/153 (1985) 603.
[36] F. Rumpf, H. Poppa, M. Boudart, Langmuir 4 (1988) 723.
[37] V.P. Zhdanov, B. Kasemo, Phys. Rev. B 55 (1997) 4105.
[38] C.R. Henry, Surf. Sci. 223 (1991) 519.
[39] D.A. King, M.G. Wells, Proc. R. Soc. London, Ser. A 339 (1974) 245.
[40] D.A. King, M.G. Wells, Surf. Sci. 29 (1972) 454.
[41] J. Libuda, PhD Thesis, Bochum, 1996.
[42] T. Engel, J. Chem. Phys. 69 (1978) 373.
[43] C.R. Henry, Surf. Sci. 223 (1989) 519.
[44] C.R. Henry, C. Chapon, C. Duriez, Z. Phys. D 19 (1991) 347.
[45] V. Matolín, I. Stará, Surf. Sci. 398 (1998) 117.
[46] T. Engel, G. Ertl, 69 (1978) 1267.
[47] I. Meusel, J. Hoffmann, J. Hartmann, M. Heemeier, M. Bäumer, J. Libuda, H.-J. Freund, Catal. Lett., submitted for publication.
[48] J. Libuda, I. Meusel, J. Hoffmann, J. Hartmann, M. Piccola, C.R. Henry, H.-J. Freund, in preparation.
[49] H. Fornander, L.-G. Ekedahl, H. Dannetun, Catal. Lett. 59 (1999) 107.
[50] H. Fornander, H. Dannetun, L.-G. Ekedahl, Surf. Sci. 440 (1999) 375.
[51] J. Miragliotta, R.S. Polizotti, P. Rabinowitz, S.D. Cameron, R.B. Hall, Appl. Phys. A 51 (1990) 221.
[52] C. Klünker, M. Balden, S. Lehwald, W. Daum, Surf. Sci. 360 (1996) 104.
[53] A. Bandara, S. Dobashi, J. Kubota, K. Onda, A. Wada, K. Domen, C. Hirose, S. Kano, Surf. Sci. 387 (1997) 312.
[54] H. Härle, A. Lehnert, U. Metka, H.R. Volpp, L. Willms, J. Wolfrum, Chem. Phys. Lett. 293 (1998) 26.
[55] F.M. Hoffmann, Surf. Sci. Rep. 3 (1983) 107.
[56] D.P. Woodruff, A.M. Bradshaw, Rep. Prog. Phys. 57 (1994) 1029.
[57] Y.R. Shen, Surf. Sci. 299/300 (1994) 551.
[58] G. Rupprechter, T. Dellwig, H. Unterhalt, H.-J. Freund, Top. Catal. (2000) in press.
[59] M. Tüshaus, W. Berndt, H. Conrad, A.M. Bradshaw, B. Persson, Appl. Phys. A 51 (1990) 91.
[60] W.K. Kuhn, J. Szanyi, D.W. Goodman, Surf. Sci. Lett. 274 (1992) L611.
[61] A.M. Bradshaw, F.M. Hoffmann, Surf. Sci. 52 (1975) 449.
[62] P. Gelin, A.R. Siedle, J.T. Yates, J. Phys. Chem. 88 (1984) 2978.
[63] D.R. Rainer, M.-C. Wu, D.I. Mahon, D.W. Goodman, J. Vac. Sci. Technol., A 14 (1996) 1184.
[64] J. Evans, B.E. Hayden, G. Lu, Surf. Sci. 360 (1996) 61.